On high-order FEM applied to canonical scattering problems in plasmonics

Mengyu Wang[1,*], Christian Engström[1,2], Kersten Schmidt[3], and Christian Hafner[1]

[1]*Laboratory for Electormagnetic Fields and Microwave Electronics, ETH Zurich, 8092, Switzerland*

[2]*Seminar for Applied Mathematics ETH Zurich, Rämistrasse 101, Zurich 8092, Switzerland*

[3]*Project POEMS (UMR CNRS/ENSTA/INRIA), INRIA Paris-Rocquencourt, 78150 Rocquencourt, France*

currently at *TU Berlin and DFG research center* MATHEON*, 10623 Berlin, Germany.*

*Corresponding author: wangm@ifh.ee.ethz.ch

June 8, 2011

Abstract

In this paper a high-order finite element method with curvilinear elements is proposed for the simulation of plasmonic structures. Most finite element packages use low order basis functions and non-curved elements, which is very costly for demanding problems such as the simulation of nano-antennas. To enhance the performance of finite elements, we use curvilinear quadrilateral elements to calculate the near-field from an impinging plane wave with second order absorbing boundary conditions. The magnetic field amplitude on the surface of one object is compared with a computation based on a multiple multipole expansion. Moreover, the convergence behavior of p-FEM with absorbing boundary conditions motivate an adaptive strategy of polynomial degree enhancement and enlargement of the domain.

Keywords: Surface Plasmon Resonance, Finite Element Method, Multiple Multipole Program, Absorbing Boundary Conditions, Curvilinear Elements, High Order Basis Functions, p-FEM.

1 Introduction

Surface plasmons may cause an enormous enhancement of the electromagnetic field in the vicinity of metallic structures [1]. This enhancement is explored in a large variety of applications including surface enhanced Raman scattering and optical antennas [2, 3, 4].

When solving Maxwell's equations in an infinite domain using finite elements, the domain must be truncated. The bounded interior region is separated from the unbounded exterior domain by an artificial boundary on which appropriate boundary conditions must be imposed to incorporate the effect of the exterior domain. The currently most popular approaches based on

differential (local) operators are perfectly matched layers (PML) [5, 6] and absorbing boundary conditions (ABC) [7]. PML can easily be extended to complicated cases, but the effect of ABC/PML parameters on the solution accuracy is better understood for ABC.

Absorbing boundary conditions have previously been used in low- and high-order finite element schemes [8, 9]. However, the rapid variation of the field at a plasmon resonance increases the computational effort necessary for obtaining a desired accuracy. Simulations of optical structures close to a plasmon resonance therefore require the development of a very efficient finite element solver.

Finite element methods are based on piecewise polynomial approximations of the solution of a partial differential equation. We can improve the quality of an approximation by a h-FEM strategy, *i. e.*, for fixed polynomial degree p, decrease the mesh size h. Alternatively, a p-FEM strategy can be used, *i. e.*, fix the mesh size h and increase the polynomial degree p. It is well known that p-FEM is superior when the solution is smooth, but a local mesh refinement is necessary in areas with very rapid variation of the field. This combination of h-refinements and p-refinements is called hp-FEM [10, 11].

We apply the Bayliss-Gunzburger-Turkel ABC (BGT) [7] to a circular artificial boundary and discretize the problem with the high order finite elements package CONCEPTS [12, 13, 14]. CONCEPTS is a C++ library supporting curvilinear elements and high polynomial basis functions, which is very efficient for achieving high accuracy [10, 11].

As test cases, we compute scattering from two geometrically simple objects; one and two silver cylinders in air. Though simple objects are used in the numerical experiments, the simulations are demanding for low order finite element methods [15]. We show the high performance of a high order finite element method with curvilinear quadrilateral elements and ABC. Our computations show that a strong plasmon resonance with a large local field enhancement can be accurately calculated with the presented method.

In order to validate our results, we need accurate reference solutions for the considered test cases. For the first case, scattering of a silver circular cylinder, the well-known Mie solution might be used [16]. As we will see later, the Mie solution can be extended to the scattering from two cylinders. However, due to severe numerical problems, highly accurate results can not be obtained with reasonable computational effort. We therefore use solutions obtained with the Multiple Multipole Program (MMP) [17, 18] as reference solutions. MMP is based on a generalization of the Mie approach that can handle arbitrary smooth geometries. For simple geometries, MMP has exponential convergence and allows solutions with machine precision as well. In the special case of a single circular cylinder, the MMP solution coincides with the Mie solution.

The paper is organized as follows. The scattering problem and the BGT boundary conditions are introduced in Section 2. The finite element formulation and CONCEPTS are described in Section 3. Numerical results are shown in Section 4 and then validated by MMP in Section 5. Finally, Section 6 concludes the paper.

2 Scattering problem and BGT conditions

The two-dimensional scattering problem is studied in this paper where the electromagnetic waves propagate in a non-magnetic material, $\mu = \mu_0$, with the relative permittivity $\epsilon(x_1, x_2) = \epsilon(\vec{x})$ independent of the third coordinate x_3.

As usual, the electromagnetic wave (E, H) is decomposed into transverse electric (TE) polarized waves $(E_1, E_2, 0, 0, 0, H_3)$ and transverse magnetic (TM) polarized waves $(0, 0, E_3, H_1, H_2, 0)$ [19]. This decomposition reduces the full 3D Maxwell equations to scalar 2D Helmholtz equations in H_3 and in E_3.

In the optical regime, a surface plasmon resonance can be excited if a noble-metal is illuminated by a transverse electric (TE) polarized wave [1]. We consider TE-waves with magnetic polarization $H(\vec{x}) = (0, 0, u)$, where u denotes the total field, and denote by k_0 the wave number of the impinging wave. The following equations characterize the scattering problem for the TE polarization,

$$\begin{aligned} -\nabla \cdot \left(\frac{1}{\epsilon(\vec{x})} \nabla u(\vec{x}) \right) - k_0^2 u(\vec{x}) = 0, \quad \vec{x} \in \Omega \\ u = u^{sc} + u^{inc}, \\ \lim_{r \to \infty} r^{1/2} \left(\frac{\partial u^{sc}}{\partial r} - \mathrm{i} k_0 u^{sc} \right) = 0, \end{aligned} \tag{1}$$

where u^{sc} and u^{inc} denote the scattered field H_3^{sc} and the incoming field H_3^{inc}, respectively.

Due to the discontinuity of the piecewise constant permittivity $\epsilon(\vec{x})$, the field will change rapidly across the material interface.

The last condition in (1) is the Sommerfield radiation condition [20], which characterizes outgoing waves. However, this condition is in the limit $r \to \infty$ and can therefore not be numerically implemented. Absorbing boundary conditions are therefore applied on the boundary of a truncated domain Ω of radius R; see Figure 1. The Bayliss-Gunzburger-Turkel (BGT) conditions are derived based on an asymptotic expansion in $k_0 R$ and are therefore accurate when $k_0 R$ is large enough [7]. The 0th to 2nd BGT conditions in polar coordinates are

$$\frac{\partial u^{sc}}{\partial r} + \alpha u^{sc} + \beta \frac{\partial^2 u^{sc}}{\partial \theta^2} = 0, \quad r, \theta \in \Gamma_0, \tag{2}$$

where the parameters α and β are given in Table 1.

3 Finite elements formulation and discretization

The computational domain Ω, see Figure 1, consists of the region of the scatterer Ω_ϵ surrounded by air Ω_0. The BGT condition is applied on the circle Γ_0 of radius R.

Following the standard procedure for the Galerkin method, the first equation in (1) is multi-

Type	α	β
BGT-0	$-ik_0$	0
BGT-1	$-ik_0 + \frac{1}{2R}$	0
BGT-2	$-ik_0 + \frac{1}{2R} - \frac{1}{8R(1-ik_0R)}$	$-\frac{1}{2R(1-ik_0R)}$

Table 1: The coefficients of the BGT absorbing boundary conditions in (2).

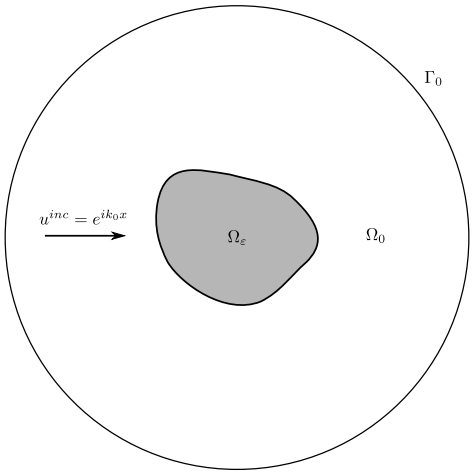

Figure 1: Computational domain Ω with the region of the scatter Ω_ϵ and artificial circular boundary Γ_0.

plied with a test function v and integrated over Ω. After integration by parts we obtain

$$\int_\Omega \frac{1}{\epsilon(\vec{x})} \nabla u \cdot \nabla v \, \mathrm{d}\vec{x} - k_0^2 \int_\Omega uv \, \mathrm{d}\vec{x} - \int_{\Gamma_0} \partial_n uv \, \mathrm{ds} = 0, \tag{3}$$

where we use the fact that Γ_0 is located outside the scatterer, which is a region of relative permittivity one, i.e, $\epsilon(\vec{x})|_{\vec{x}\in\Gamma_0} = 1$.

We apply second order ABC (2) to the total field u. The condition on the circular artificial boundary then takes the form

$$\partial_n u = \left(-\alpha u - \beta \frac{\partial^2 u}{\partial \theta^2}\right) + \left(\alpha u^{inc} + \partial_n u^{inc} + \beta \frac{\partial^2 u^{inc}}{\partial \theta^2}\right). \tag{4}$$

From (3) and (4) it follows that the variational formulation of TE scattering problems with the BGT boundary condition is as follows: Find a function u such that

$$a(u, v) = b(v), \tag{5}$$

holds for all test functions v, where the sesquilinear form $a(u, v)$ and the linear form $b(v)$ are

$$a(u, v) = \int_\Omega \left(\frac{1}{\epsilon(\vec{x})} \nabla u \cdot \nabla v - k_0^2 uv\right) \mathrm{d}\vec{x} + \int_{\Gamma_0} \left(\alpha uv + \beta \frac{\partial^2 u}{\partial \theta^2} v\right) \mathrm{ds}, \tag{6}$$

and

$$b(v) = \int_{\Gamma_0} \left(\alpha u^{inc} + \partial_n u^{inc} + \beta \frac{\partial^2 u^{inc}}{\partial \theta^2}\right) v \,\mathrm{ds}. \tag{7}$$

We refer to [21] for a more detailed mathematical description of the variational problem (5).

The edge integral $\int_{\Gamma_0} \frac{\partial^2 u}{\partial \theta^2} v \,\mathrm{ds}$ can not be implemented directly. However, due to the fact that Γ_0 is closed, integration by parts gives

$$\int_{\Gamma_0} \frac{\partial^2 u}{\partial \theta^2} v \,\mathrm{ds} = -\int_{\Gamma_0} \frac{\partial u}{\partial \theta} \frac{\partial v}{\partial \theta} \,\mathrm{ds} + 0. \tag{8}$$

On the circular boundary Γ_0, the tangential derivative is

$$\frac{\partial}{\partial \theta} = R \frac{\partial}{\partial s}.$$

Therefore the edge integral becomes

$$\int_{\Gamma_0} \frac{\partial^2 u}{\partial \theta^2} v \,\mathrm{ds} = -\int_{\Gamma_0} R^2 \frac{\partial u}{\partial s} \frac{\partial v}{\partial s} \,\mathrm{ds}.$$

If one chooses an absorbing boundary on a curve other than a circle, *e. g.*, an ellipse, the formulation and implementation will be more complicated [22, 23]. Despite of this, the elliptic absorbing boundary is more efficient than the circular one for long shape scatterers. In this paper, we only apply ABC on a circular absorbing boundary, which is sufficient for the problems under study.

For the discretization of (5) we use the C++ library CONCEPTS [12, 13, 14] (www.concepts.math.ethz.ch). The CONCEPTS package uses high polynomial basis functions and curved quadrilateral elements. We use curved elements because its edges can resolve the

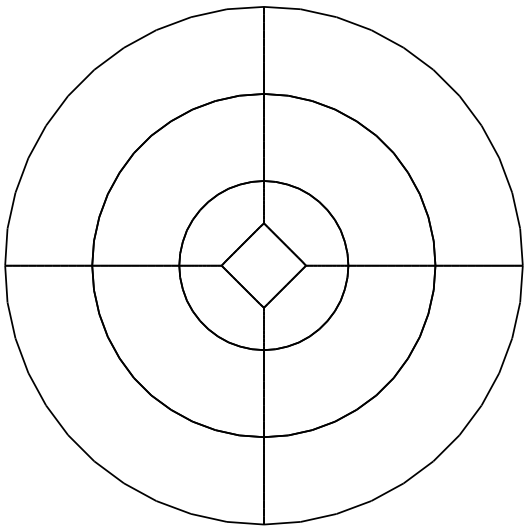

Figure 2: CONCEPTS mesh with 13 curved quadrilateral cells used in the p-FEM computations with CONCEPTS.

circular material interface exactly. As a result, the quadrature points of the high polynomial basis follow the material interface by which the approximation order of the high order polynomial basis is retained. Figure 2 shows the CONCEPTS mesh, which contains 13 curved quadrilateral elements. We use the p-FEM strategy, which means the higher accuracy is obtained by increasing the orders of the basis functions [10]. The basis functions of each order are constructed as products of 1D basis functions based on Jacobi polynomials in both directions of the reference square $[0, 1]^2$, which are then mapped to the physical element in the mesh [24, Chapter 9] or [25]. Then, the matrix entries are computed by numerical quadrature on the reference square. Note, that the used basis distinguish itself by moderate matrix conditioning [26]. Similar bases can be constructed for (vectorial) edge elements on quadrilaterals and hexahedra for full Maxwell systems [27].

In all computations we have used the direct solver SuperLU [28]. A direct solver can be used for larger systems with p-FEM than with h-FEM as the number of degrees of freedom remains moderate for high accuracy. For very large problems, especially in 3D, iterative solvers are potentially more efficient.

Many finite element packages and commercial softwares use linear or quadratic basis functions on triangular meshes such as in Figure 3, which is generated by FreeFEM++ (www.freefem.org/ff++). With this limited set of basis functions, higher accuracy is obtained by making the mesh finer while keeping the order of the basis functions fixed. This strategy is called h-FEM [10]. Often the non-curved elements are used, where the curved interfaces are resolved by discretization with more elements.

Using h-FEM with linear or quadratic basis functions leads to a low algebraic convergence in the number of degrees of freedom. This is in contrast with a p-FEM strategy with curved elements which gives exponential convergence for piecewise smooth solutions [13, 10], in the

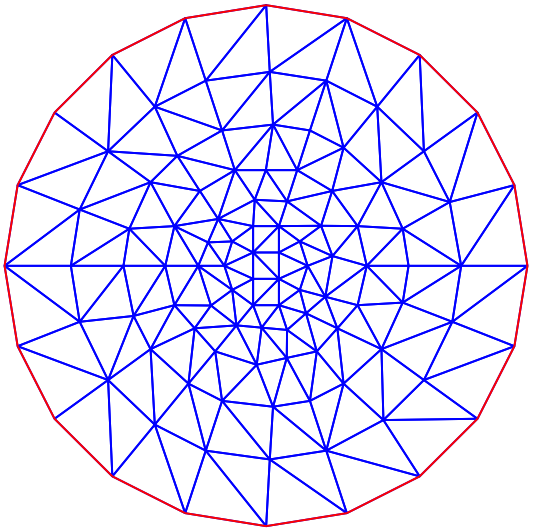

Figure 3: Example of triangular mesh generated by FreeFEM++.

number of degrees of freedom, the number of nonzero entries in the system matrix as well as the computation time. The system matrices for p-FEM are less sparse than for h-FEM. If the mesh includes mainly non-parallelogramme cells, the ratio of the number of non-zero and the total number matrix entries depends only on the number of cells, and does not decrease when p increases.The reason is that for non-parallelogramme cells, for example generally curved cells, the orthogonality relation derived on the reference element does not transform to the physical cell. Nevertheless, to achieve the same accuracy the number of degrees of freedom for h-FEM increase much faster than for p-FEM, leading to the fact that p-FEM works with smaller, but more dense populated matrices. This issue will be demonstrated in detail in Section 4.3.

4 Numerical results and discussions

4.1 Scattering from one cylinder

We compute the scattering from a silver circular wire illuminated by an incoming plane wave at an optical frequency. The problem was previously studied in [15], where the performance of low-order finite elements was compared with several integral equation based solvers. In the numerical experiments, we implement the second order BGT boundary condition in CONCEPTS and use high order curvilinear elements.

The geometry and the material model are taken from [15], *i. e.*, silver is characterized as a homogenous material described by the Drude Model [19, 29]:

$$\begin{aligned} \epsilon(\omega) &= \epsilon_\infty - \frac{\omega_p^2}{\omega(\omega + i\Gamma)}, \\ \epsilon_\infty &= 5,\ \omega_p = 1.4433 \times 10^{16} \text{ rad/s},\ \Gamma = 10^{14} \text{ rad/s}. \end{aligned} \tag{9}$$

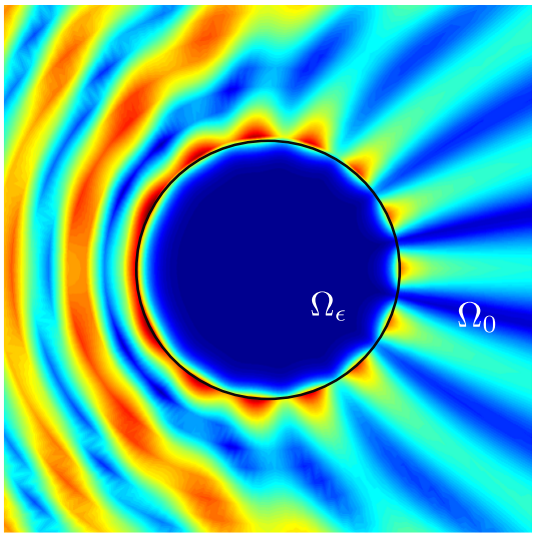

Figure 4: The absolute value of total magnetic field, with 2596 degree of freedom. The radius of the silver wire is 400nm, and the wavelength is 413nm. The permittivity of silver -5.0092942+0.2194588i, is calculated from the Drude model (9). A strong surface plasmon resonance is observed.

At wavelength 413nm, (9) gives that the permittivity of silver is $-5.00929 + 0.21946i$.

We first compute the scattering from one cylinder of radius 400nm, with the mesh of 13 curvilinear elements shown in Figure 2. The second order BGT boundary condition is set on Γ_0, which is located two wavelengths away from the scatterer. The polynomial degree of the basis is 15, resulting in 2596 degrees of freedom. The absolute value of the total magnetic field is shown in Figure 4, where one can observe a strong surface plasmon resonance on the surface of the scatterer.

The strong resonance is due to the large negative real part and small positive imaginary part, which result in a strong surface plasmon resonance [15].

To validate the FEM results, we compare the field values along the surface of the cylinder with those obtained from MMP, which coincides with the analytical Mie solution and provides a solution with machine precision when the number of multipole and Bessel orders is high enough. The required order depends on the radius of the cylinder, its material properties, and on the wavelength. Because of the exponential convergence and internal error checking capabilities of MMP, one easily may find the required multipole order. Since the cylinder considered in the test case is rather large, quite high orders are required. For maximum multipole order 27, the MMP solution has 56 degrees of freedom and reaches in average a relative error below $1.2 \times 10^{-13}\%$, *i. e.*, machine precision is reached. For maximum order $>$27 almost the same error is obtained, *i. e.*, the error does not decrease further for higher multipole orders. Note that the highest errors are usually obtained in the close vicinity of the interface between two different materials. Therefore, the comparison of the field values on the surface of the cylinder is a much harder test than, for example, a comparison of the far field. It should be also mentioned that the relative error is usually the highest at points where the field is rather weak. Thus, the maximum

relative errors may be considerably higher than the average relative errors. In the considered test case, the maximum relative error is below $4 \times 10^{-13}\%$, *i. e.*, also very low, which provides high confidence in the reference results.

The comparison between CONCEPTS and MMP is shown in Figure 5. A very good agreement is achieved with only 2956 degrees of freedom and therefore very little computational effort. Notice that the degrees of freedom in MMP and finite elements can not directly be compared since discretization with MMP results in full matrices whereas the FE discretization results in sparse matrices. Compared with low order non-curved finite elements, high order basis functions with curved elements are more efficient for problems with curved material interfaces.

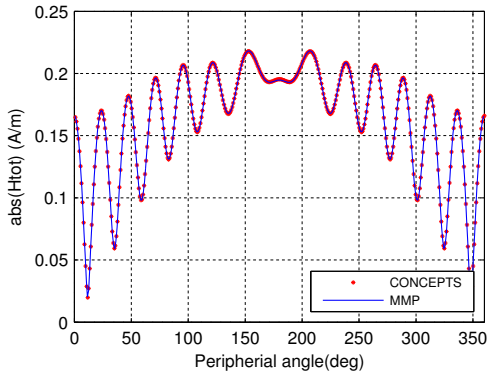

Figure 5: The comparison of $|\mathrm{H}^{\mathrm{total}}|$ across the material interface, between CONCEPTS results and MMP results. The mesh is shown in figure 2 with the degrees of freedom 2956, and the absorbing boundary is 2λ away from the scatterer.

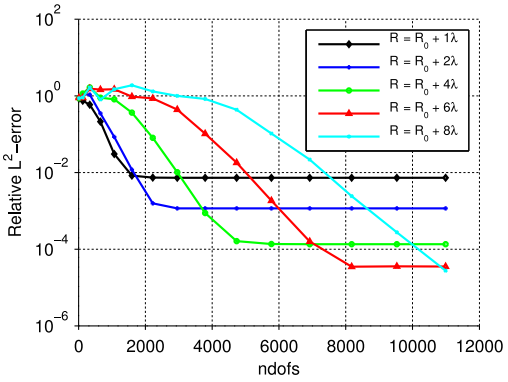

Figure 6: p-FEM convergence. The distance between the boundary and the scatterer is 1,2,4,6, and 8 times of the wavelength, respectively.

With the mesh fixed, we increase the order of basis function to study the p-FEM convergence. The relative L^2 error is computed within the region Ω_E of radius $R_0 + 2/3\lambda$. That is, we compute

the ratio between the L^2 norm of $u - u_{ref}$ and u_{ref}:

$$\text{relative } L^2 \text{ error} = \frac{\sqrt{\int_{\Omega_E} |u - u_{ref}|^2 d\vec{x}}}{\sqrt{\int_{\Omega_E} |u_{ref}|^2 d\vec{x}}},$$

where u_{ref} denotes the MMP reference solution. The reasons of taking relative L^2-error only in the near field region Ω_E are twofold: Firstly, one can compute the far-field information from the near-field pattern, secondly, for the plasmonic devices, the near field behavior is of high interest.

We study the problem with different radii of the absorbing boundary. For each radius, the p-convergence is studied. We increase the polynomial degree of the basis from 1 to 29 with an increment of 2. For each step, the relative L^2 error is computed, and the degrees of freedom and the consumed time are recorded. We perform these simulations using one core of a 4×2.4GHz Intel quad-core machine, with 8GB RAM. The final test of polynomial degree 29 uses 10992 degrees of freedom, and takes 326 seconds. The convergence results are shown in Figure 6, where one can observe the following properties:

For low degrees of freedom the relative error remains practically at 100 %. In this range the wave is resolved with less than 3 degrees of freedom per wavelength and utterly wrong. This phase with low accuracy is longer if the computational domain is larger. However, when a certain minimum resolution is reached a fast convergence follows [30], with more rapid convergence for a smaller computational domain. Finally, the convergence stops at a limited accuracy, which is determined by the radius of the absorbing boundary and can be explained as the model limitation of the asymptotic expansion in the BGT condition. This is a drawback compared with PML, where the absorbing layers can be placed very close to the scatterer, however, for the price of more degrees of freedom to model the PML layer. Recent research shows that high-order ABC may have favorable complexity estimates relative to PML [31].

We observe that a higher accuracy can be reached if the absorbing boundary is put further away from the scatterer. This is a consequence of the asymptotic nature of the BGT conditions [7], for which the error decays with the radius and for increasing wave numbers. However, there is a trade-off between the higher model accuracy and the higher computational complexity of a larger computational domain. If the absorbing boundary is further away, the convergence will be slower, since more degrees of freedom are consumed to resolve the solution in free space. This tells us that the accuracy of a numerical solution can be improved by enlarging the computational domain, and as a result, the computational costs will increase as well.

This observation also suggest that we would benefit from using an adaptive strategy. One can follow the fast convergence of a small computational domain at the beginning, then after the convergence stops, increase the domain size for a further convergence to reach a better accuracy. This algorithm behaves like a tracing strategy, finding the bottom in the convergence plot in Figure 6. However, this is not easy for arbitrary problems, where the solution is unknown. Then one must find a way to know when the convergence slows down.

In order to find the factors that influence the efficiency of the numerical method and using ABC, we compute the relative L^2 errors with respect to the time consumption. We first use the mesh in Figure 2 and then a finer mesh in Figure 7, which is obtained after one step uniform h-

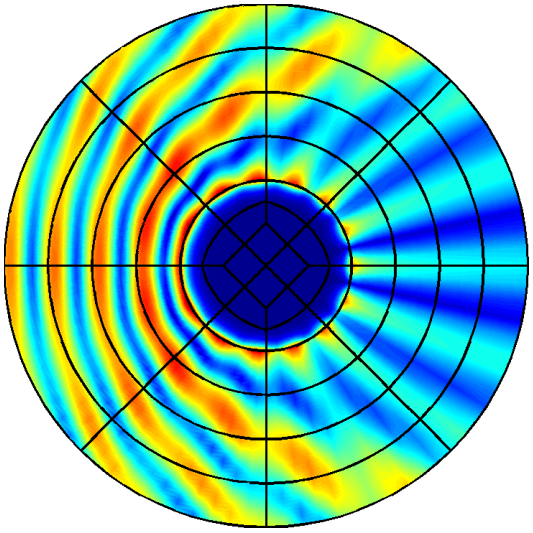

Figure 7: A finer mesh and the solution. This mesh, consisting of 52 elements, is obtained after one step uniform h-refinement based on the mesh in Figure 2.

refinement of the mesh in Figure 2, and has therefore four times more elements. The convergence plots with respect to the time indicating the efficiency are shown in Figure 8.

We observe that the errors decay faster for the finer mesh when increasing the polynomial degree. In fact with the finer mesh the same error is obtained with smaller polynomial degrees, and that for lower computational cost. For example the green curves in Figure 8 stop at the same error level indicating the modelling error of the ABC with outer radius $R_0 + 4\lambda$. For the coarse mesh this saturation level is reached with $p = 19$ (and 4732 degrees of freedom) and with a computation time $t = 36\,\mathrm{s}$, whereas it is reached for the finer mesh already with $p = 11$ (and 6337 degrees of freedom), but within $t = 8.4\,\mathrm{s}$ only. The reasons of the higher computational effort per degree of freedom is the lower sparsity of the system matrices when using high polynomial degrees on a coarser mesh. More basis functions overlap than with lower polynomial degrees on a finer mesh. This lower sparsity would be less emphasized when we would have used non-curved trapezoidal or even parallelogram shaped elements due to orthogonality of a larger number of basis functions. The lower computational effort for finer meshes and lower polynomial degrees is punished with a lower asymptotic convergence rate, which is not visible in our example as the accuracy is limited by the ABC.

4.2 Scattering from two cylinders

The scattering of two cylinders is a more demanding problem than that of one cylinder, namely because the gap is very narrow with respect to the radius of the cylinders, which makes the meshing difficult and causes a strong plasmonic interaction with a very high field enhancement in the gap area. The latter is attractive for practical applications. This strong interaction has also an impact on the analytic Mie solution. Theoretically one may model the scattered field with two multipole expansions, located in the centers of the two cylinders. Furthermore, one

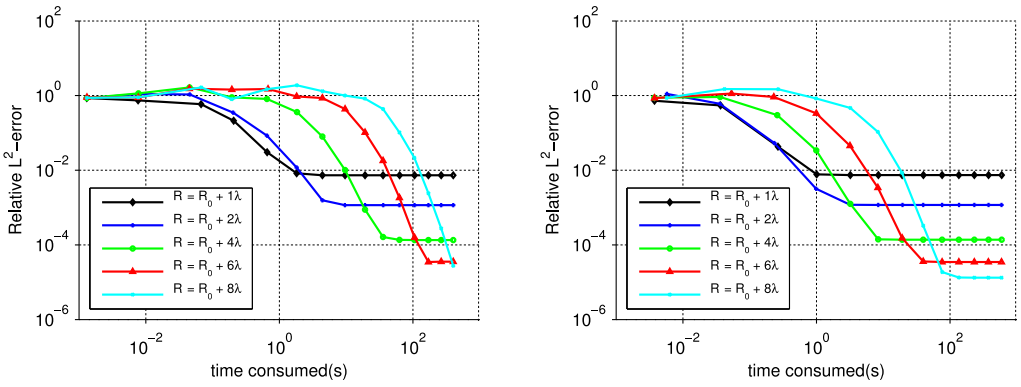

Figure 8: The relationship between computation time and relative L^2 error from scattering of one cylinder: (a) with the mesh shown in Figure 2, and (b) with the finer mesh in Figure 7.

may model the field inside each cylinder by a Bessel expansions as for the single cylinder case. This extended Mie solution should also converge exponentially because the boundaries of the cylinders are still circular. However, exponential convergence does not mean that the multipole order required to obtain machine precision is low or even similar to the order required for the single cylinder case. It turns out that severe numerical problems occur due to cancellation effects and in the computation of high multipole and Bessel orders. Therefore, one cannot even reach a reasonable accuracy of a few digits when double precision numerics is used. MMP now offers the opportunity to account for the strong interaction by placing additional multipoles located near the gap area. Furthermore, one may take the symmetry into account. Then one must model only one of the two cylinders explicitly. With two "auxiliary" multipoles located near the gap, in addition to a multipole and Bessel expansion located in the center of the cylinder. One then reaches machine precision with multipole order 45, *i. e.*, 364 degrees of freedom.

In the finite element computation, we implement a second order BGT condition, which is put eight wavelengths away from the scatterer. The absolute value of the total magnetic field is shown in Figure 9, where one can observe strong local field enhancement in between the gap. There is no analytical solution for this problem. Therefore MMP is a valuable source for generating reliable reference solutions. In Figure 10, the comparison of $|\mathrm{H}^{\mathrm{total}}|$ across the material interface of the upper cylinder is shown, where a very good agreement is achieved. However, unlike the one cylinder scattering, the computation is not cheap. We compute on an i7-980X Intel machine with 24GB RAM, using 13409 degrees of freedom. Using one core, the computation time is 17.4 seconds to achieve the accuracy in Figure 10.

As for the one cylinder problem, the convergence behavior is studied for two cylinders case. The relative L^2 error is computed on Γ, which is the material interface of the upper cylinder.

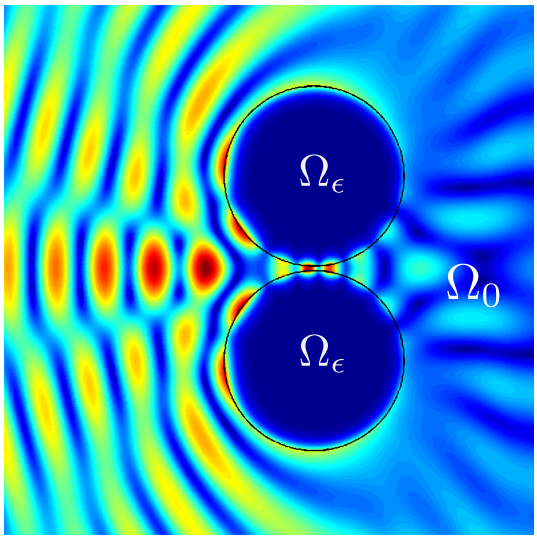

Figure 9: The absolute value of total magnetic field. The radius of the silver wire is 400nm and the gap between the two wires is 20nm, with incoming wave of wavelength 413nm. A strong local enhancement can be observed in between the gap.

That is, we compute the ratio between the L^2 norm of $u - u_{ref}$ and u_{ref}:

$$\text{relative } L^2 \text{ error} = \frac{\sqrt{\int_\Gamma |u - u_{ref}|^2 d\vec{x}}}{\sqrt{\int_\Gamma |u_{ref}|^2 d\vec{x}}},$$

where u_{ref} denotes the MMP reference solution. The convergence results are shown in Figure 11.

Firstly, we study the p-convergence for different sizes of the absorbing boundary, and the results are shown as solid lines in the figure. We can observe similar properties as in the scattering problem for one cylinder.

Secondly, in order to compare between p-FEM and h-FEM, we perform an h-convergence analysis. The absorbing boundary is put 4λ away from the scatterer and we use quadratic curvilinear finite element, which is commonly used in commercial and scientific softwares. The result is shown as the dashed line in the figure and it is obviously that for this problem, p-FEM converges faster than h-FEM and consumes less degrees of freedom. Moreover, CONCEPTS was recently compared with FreeFEM++, which uses non-curved triangular elements [32]. This comparison shows the importance of using curved elements.

4.3 Further discussion

Sparsity and condition number

It is important to study the sparsity and the condition number for matrices resulting from discretization with high order cuvilinear finite elements [21]. We choose two computation exam-

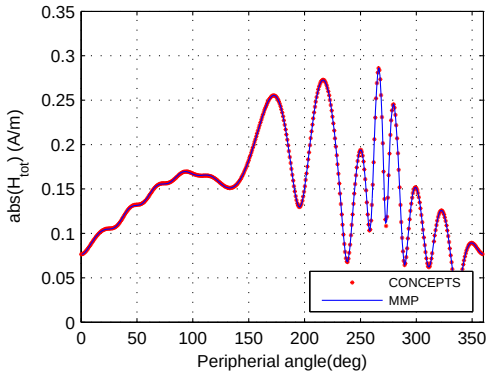

Figure 10: The comparison between MMP and CONCEPTS results of $|\mathrm{H}^{\mathrm{total}}|$ in the two cylinders case, the values are taken across the the material interface of the upper cylinder. The absorbing boundary is 4λ from the scatter, and the computation consumes 13409 degrees of freedom.

ples of similar accuracies in Figure 11: test case A is obtained by 5 steps of h-refinement with degrees of freedom 213377, and reaches accuracy 0.012, while test case B is obtained by 10 steps of p-refinement with degrees of freedom 20921, and reaches accuracy 0.0076. The system matrices structures are shown in Figure 12, from which we can observe that the matrices in both cases are sparse. The density, *i. e.*, the retio between the number of nonzero matrix entries and the total number of matrix entries, of the matrices A is 9.3×10^{-5} for case A, and 6.8×10^{-3} for case B. The condition numbers are 9.25×10^5 for case A, and 9.75×10^5 for case B, which are both very low. The high sparsity and low condition number imply that high order curvilinear finite element will also have good performance in large 2D and 3D problems.

The situation of MMP is different. Like all boundary discretization methods, MMP leads to relatively small but full matrices that tend to be ill-conditioned. MMP works with an overdetermined system of equations and special procedures that can provide highly accurate results even when the condition numbers of the MMP matrices are higher than 10^{16}. The efficiency of MMP and similar boundary discretization methods is higher for low dimensions and increases with the smoothness of the interfaces. Therefore, MMP is highly attractive for 2D problems with not too complex geometry and for 3D problems with sufficiently smooth geometry. Thus, MMP is excellent for delivering reference solutions for scattering from objects with smooth interfaces. However, for 2D problems with complicated geometry and most of the 3D problems, FEM is more efficient then MMP.

hp-Adapativity

The computational cost can significantly be reduced with an hp-adaptivity [11]. Different strategies should be applied to different regions. Due to the surface plasmon resonance, the field concentrates along the material interfaces. Thus it is very week and varies slowly deep inside the scatterer. This part can therefore be modeled using big elements with low order polynomials. Secondly, the field along the surface varies very rapidly, which suggest that an h-refinement

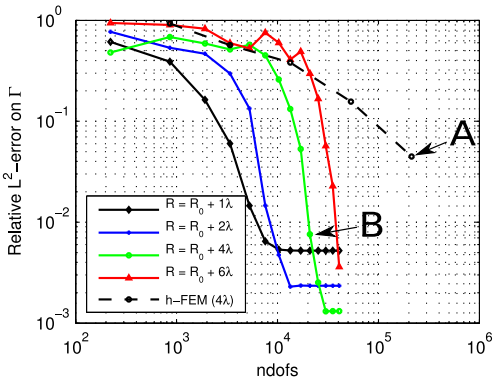

Figure 11: Convergence for the two cylinders case. The solid lines represent the p-convergence for the boundary 1,2,4, and 6λ away from the scatterer, respectively. The dashed line represents the h-convergence for the boundary 4λ away from the scatterer, using quadratic curvilinear finite elements. A and B are two computation examples in Section 4.3.

strategy may be favourable. Finally, the field in free space at some distance from the surface is smooth. Therefore a p-refinement strategy should be applied there.

Extension to problems in 3D

The presented study for scattering on geometries with very small gaps was in 2D, where despite the very low error levels the computational effort remains moderately. For rotational symmetric situations in 3D, a Fourier decomposition of the incoming field can be applied and for each Fourier component a vectorial problems in a 2D plane has to be solved, where again quadrilateral meshes can be used. In this case, the high-order version of the so-called edge elements [33] can be used, which represent vectorial fields with tangential continuity over the cell boundaries. These edge elements of high-order can be implemented, *e. g.*, with a similar basis based on Jacobi polynomials to keep moderate matrix conditioning, where for quadrilaterals the definition is especially simple as each vector component is a tensor-product of one-dimensional basis functions. Also for general 3D configurations high order 3D edge elements on hexahedral cells have been introduced [27].

5 Conclusions and outlook

We have studied 2D canonical scattering problems in plasmonics, with finite elements and the BGT absorbing boundary conditions. We use CONCEPTS to implement the 0th to 2nd BGT conditions. CONCEPTS is a C++ library using high order finite elements and curved quadrilateral cells, which provides results with high accuracy and efficiency. To validate the results, we use MMP, which may be considered as a semi-analytic approach that can reach machine precision for smooth objects such as circular cylinders. An excellent agreement between MMP and

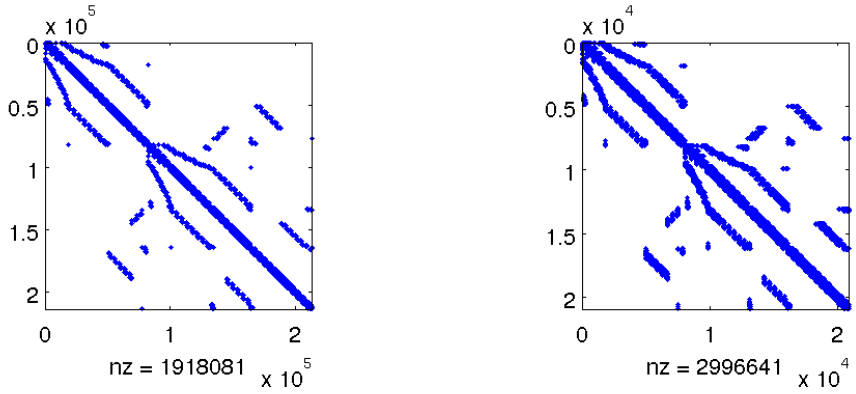

Figure 12: The structure of the system matrices: (a) for test example A in Figure 11, (b) for test example B in Figure 11.

CONCEPTS was reached with quite small computational effort.

The behavior of the BGT absorbing boundary conditions are then studied. BGT conditions are derived based on an asymptotic expansion in k_0R, as a result, there is a limitation of the model for a fixed domain size. The closer the boundary is placed, the faster the convergence of p-FEM. However, the model error of the BGT condition increases when the artificial boundary is put closer to the cylinder(s), which finally dominates the overall error. This behavior implies that an adaptive strategy of polynomial degree enhancement and enlargement of the computational domain should be developed.

Moreover, we study scattering of two cylinders with a very narrow gap, which is much more demanding than scattering of one cylinder. Nevertheless, the proposed method achieves on a mesh with small cells close to the narrow gap similar results as for the single cylinder. We compare the p-FEM to h-refinement with polynomial degree 2, where we observe much faster convergence with the discretisation of high orders. As p-FEM is per degree of freedom more costly, it is in some situations more efficient to refine the coarse mesh once or even several times before the use of p-FEM with its exponential convergence accounts for.

The complex structure of the near field in the vicinity of plasmonic structures motivates to use an hp-adaptivity strategy to use small cells with low polynomial degrees in regions with fast variations and large cells with high polynomial degrees in regions with slow variations. Another interesting issue is the comparison of the performance between ABC and PML. A PML based code is now under development using CONCEPTS. The comparison will be presented elsewhere.

Acknowledgments

The first author acknowledges the support of the Swiss National Science Foundation (SNSF 119813).

References

[1] Y. Fang, N. Seong, and D. Dlott, "Measurement of the distribution of site enhancements in surface-enhanced Raman scattering," *Science*, vol. 321, no. 5887, p. 388, 2008.

[2] H. Xu, E. Bjerneld, M. Käll, and L. Börjesson, "Spectroscopy of single hemoglobin molecules by surface enhanced Raman scattering," *Physical review letters*, vol. 83, no. 21, pp. 4357–4360, 1999.

[3] S. Nie and S. Emory, "Probing single molecules and single nanoparticles by surface-enhanced Raman scattering," *Science*, vol. 275, no. 5303, p. 1102, 1997.

[4] L. Novotny and B. Hecht, *Principles of nano-optics*. Cambridge, UK: Cambridge Univ Press, 2006.

[5] J. P. Berenger, "A perfectly matched layer for the absorption of electromagnetic waves," *Journal of Computational Physics*, vol. 114, pp. 185–200, 1994.

[6] P. Monk and F. Collino, "The perfectly matched layer in curvilinear coordinates," *SIAM J. Sci. Comput*, vol. 19, pp. 2061–2090, 1996.

[7] A. Bayliss, M. Gunzburger, and E. Turkel, "Boundary conditions for the numerical solution of elliptic equations in exterior domains," *SIAM J. Appl. Math.*, vol. 42, no. 2, pp. 430–451, 1982.

[8] J. Shirron and I. Babuška, "A comparison of approximate boundary conditions and infinite element methods for exterior Helmholtz problems," *Computer Methods in Applied Mechanics and Engineering*, vol. 164, no. 1-2, pp. 121–139, 1998.

[9] C. Engström, "On a high-order discontinuous galerkin method applied to canonical scattering problems," in *International Symposium on Electromagnetic Theory (EMTS 2010), Berlin, Germany*, August 16– 19 2010, pp. 907–910.

[10] C. Schwab, *p- and hp- Finite Element Methods: Theory and Applications in Solid and Fluid Mechanics*. Oxford, UK: Oxford University Press, 1998.

[11] L. Demkowicz, *Computing with Hp-adaptive Finite Elements: One and two dimensional elliptic and Maxwell problems*. Boca Raton, USA: CRC Press, 2006.

[12] P. Frauenfelder and C. Lage, "Concepts—an object-oriented software package for partial differential equations," *Math Model Numer Anal.*, vol. 36, no. 5, pp. 937–951, 2002.

[13] K. Schmidt and P. Kauf, "Computation of the band structure of two-dimensional photonic crystals with *hp* finite elements," *Comput. Methods Appl. Mech. Engrg.*, vol. 198, pp. 1249–1259, 2009.

[14] K. Schmidt and R. Kappeler, "Efficient computation of photonic crystal waveguide modes with dispersive material," *Optics Express*, vol. 18, no. 7, pp. 7307–7322, 2010.

[15] J. Smajic, C. Hafner, L. Raguin, K. Tavzarashvili, and M. Mishrikey, "Comparison of numerical methods for the analysis of plasmonic structures," *J. Comput. Theor. Nanosci*, vol. 6, pp. 1–12, 2009.

[16] W. Sun, N. Loeb, and B. Lin, "Light scattering by an infinite circular cylinder immersed in an absorbing medium," *Applied optics*, vol. 44, no. 12, pp. 2338–2342, 2005.

[17] C. Hafner, *MaX-1: a visual electromagnetics platform for PCs*. Chichester, UK: John Wiley & Sons, 1999.

[18] ——, *Post-modern electromagnetics: using intelligent Maxwell solvers*. Wiley, 1999.

[19] J. D. Jackson, *Classical Electrodynamics*, 3rd ed. New York: John Wiley & Sons, 1999.

[20] A. Sommerfeld, *Partial differential equations in physics*. New York: Academic Press, 1949.

[21] F. Ihlenburg, *Finite element analysis of acoustic scattering*. Berlin: Springer-Verlag, 1998.

[22] C. Lee, R. Shin, J. Kong, and B. McCartin, "Absorbing boundary conditions on circular and elliptical boundaries," *Journal of Electromagnetic Waves and Applications*, vol. 4, no. 10, pp. 945–962, 1990.

[23] H. Barucq, R. Djellouli, and A. Saint-Guirons, "Performance assessment of a new class of local absorbing boundary conditions for elliptical- and prolate spheroidal-shaped boundaries," *Applied Numerical Mathematics*, vol. 59, no. 7, pp. 1467–1498, 2009.

[24] K. Schmidt, "High-order numerical modeling of highly conductive thin sheets," PhD thesis, ETH Zurich, Zürich, July 2008.

[25] G. E. Karniadakis and S. J. Sherwin, *Spectral/hp Element Methods for Computational Fluid Dynamics*. Oxford, UK: Oxford University Press, 2005.

[26] P. Frauenfelder, "hp-finite element methods on anisotropically, locally refined meshes in three dimensions with stochastic data," PhD thesis, ETH Zurich, Zürich, 2004. [Online]. Available: http://e-collection.ethbib.ethz.ch/view/eth:27514

[27] M. Ainsworth and J. Coyle, "Conditioning of hierarchic p-version Nédélec elements on meshes of curvilinear quadrilaterals and hexahedra," *SIAM Journal on Numerical Analysis*, vol. 41, no. 2, pp. 731–750, 2004.

[28] J. W. Demmel, S. C. Eisenstat, J. R. Gilbert, X. S. Li, and J. W. H. Liu, "A supernodal approach to sparse partial pivoting," *SIAM J. Matrix Analysis and Applications*, vol. 20, no. 3, pp. 720–755, 1999.

[29] C. Hafner, "Drude model replacement by symbolic regression," *Journal of Computational and Theoretical Nanoscience*, vol. 2, no. 1, pp. 88–98, 2005.

[30] M. Ainsworth, "Discrete dispersion relation for hp-version finite element approximation at high wave number," *SIAM Journal on Numerical Analysis*, vol. 42, no. 2, pp. 553–575, 2005.

[31] T. Hagstrom, T. Warburton, and D. Givoli, "Radiation boundary conditions for time-dependent waves based on complete plane wave expansions," *Journal of Computational and Applied Mathematics*, vol. 234, no. 6, pp. 1988–1995, 2010.

[32] C. Engström, C. Hafner, and K. Schmidt, "Computations of lossy bloch waves in two-dimensional photonic crystals," *J. Comput. Theor. Nanosci.*, vol. 6, pp. 775–783, 2009.

[33] M. Ainsworth and J. Coyle, "Hierarchic hp-edge element families for Maxwell's equations on hybrid quadrilateral/triangular meshes," *Comp. Meth. App. Mech. Engr.*, vol. 190, no. 49, pp. 6709–6733, October 2001.